REPORT DOCUMENTATION PAGE

Form Approved OMB No. 0704-0188

1. REPORT DATE *(DD-MM-YYYY)*	2. REPORT TYPE	3. DATES COVERED *(From – To)*
	Final Report	16 December 2004 - 16-Dec-05

4. TITLE AND SUBTITLE

Planar Magneto-Inductive Waveguide Devices

5a. CONTRACT NUMBER
FA8655-05-1-3007

5b. GRANT NUMBER

5c. PROGRAM ELEMENT NUMBER

6. AUTHOR(S)

Professor Richard R Syms

5d. PROJECT NUMBER

5d. TASK NUMBER

5e. WORK UNIT NUMBER

7. PERFORMING ORGANIZATION NAME(S) AND ADDRESS(ES)
Imperial College London
Exhibition Road
London SW7 2AZ
United Kingdom

8. PERFORMING ORGANIZATION REPORT NUMBER

N/A

9. SPONSORING/MONITORING AGENCY NAME(S) AND ADDRESS(ES)

EOARD
PSC 802 BOX 14
FPO 09499-0014

10. SPONSOR/MONITOR'S ACRONYM(S)

11. SPONSOR/MONITOR'S REPORT NUMBER(S)
SPC 05-3007

12. DISTRIBUTION/AVAILABILITY STATEMENT

Approved for public release; distribution is unlimited.

13. SUPPLEMENTARY NOTES

14. ABSTRACT

This report results from a contract tasking Imperial College London as follows: The Grantee will perform theoretical analysis and experimental investigations of simple planar magneto-inductive wave circuits based on closely coupled LC resonators and formed using low cost flexible PCB techniques. The aim will be to establish propagation characteristics, investigate coupling to electromagnetic radiation in straight sections and bends and demonstrate magnetic field concentration.

15. SUBJECT TERMS
EOARD, Electromagnetic Fields, radar, Antennas

16. SECURITY CLASSIFICATION OF:			17. LIMITATION OF ABSTRACT	18, NUMBER OF PAGES	19a. NAME OF RESPONSIBLE PERSON
a. REPORT	b. ABSTRACT	c. THIS PAGE			MICHAEL KJ MILLIGAN, Lt Col, USAF
UNCLAS	UNCLAS	UNCLAS	UL	41	19b. TELEPHONE NUMBER *(Include area code)* +44 (0)20 7514 4955

Planar Magneto-Inductive Waveguide Devices

Final Report to EOARD

by

R.R.A.Syms, L.Solymar and I.R.Young,

EEE Dept., Imperial College London,

Exhibition Road, London, SW7 2AZ, UK

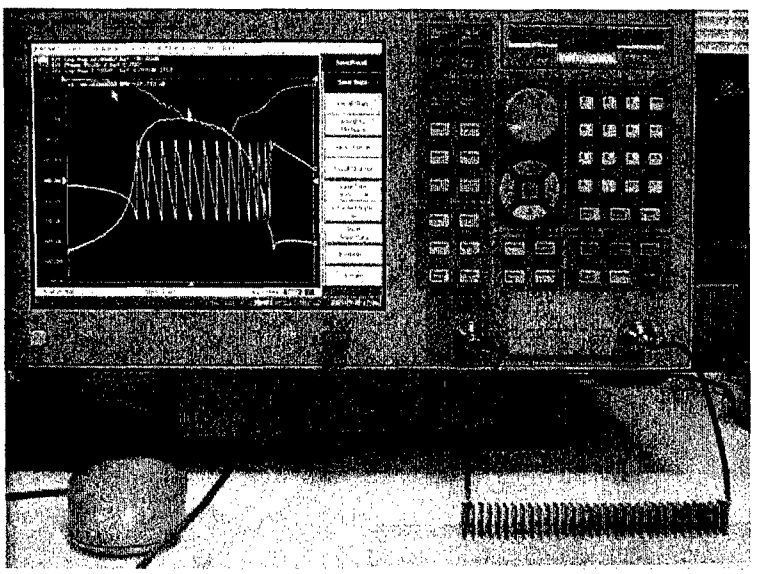

1. Introduction

Magneto-inductive (MI) waves are a new type of predominantly magnetic wave that can propagate in chains of magnetically coupled resonant structure [1-4]. The aim of this report is to describe experimental work on MI waves carried out at Imperial College London under the USAF sponsored project FA8655-05-1-3007 "Planar magneto-inductive waveguide devices". The aims are to demonstrate the propagation of magneto-inductive waves using a simple low-frequency experimental test-bed, to establish accurate methods for determining propagation characteristics and to investigate possibilities for quasi-optical MI devices.

2. Theoretical background

We first give a brief theoretical background, and derive the dispersion characteristic of MI waves under several different conditions.

2.1 Dispersion characteristic for nearest neighbour coupling

Figure 1a shows the geometry of a MI waveguide supporting forward waves. The structure consists of a set of regularly spaced L-C resonators, and Figure 1b shows the lumped element equivalent circuit for low frequency operation. Assuming that the coupling is restricted to nearest-neighbours, the currents I_n, I_{n+1} and I_{n-1} in three neighbouring elements can be shown using Kirchoff's law to be related by:

$$\{R + j\omega L + 1/j\omega C\}I_n + j\omega M\{I_{n+1} + I_{n-1}\} = 0 \quad (1)$$

Here $\omega = 2\pi f$ is the angular frequency, R and L and the resistance and inductance of each element, C is the capacitance, and M is the mutual inductance. Assuming a travelling wave

solution $I_n = I_0 \exp(-jka)$, where k is the propagation constant, we obtain:

$$\{1 - \omega_0^2/\omega^2 - j/Q\} + \kappa \cos(ka) = 0 \tag{2}$$

Here $Q = \omega L/R$ is the quality factor (or Q-factor) and $\kappa = 2M/L$ is the coupling coefficient. For positive κ, the waveguide supports forward waves. Figure 1c shows the alternative planar configuration, for which κ is negative. This geometry supports backward waves.

Assuming now that k is complex, so that we may write $k = k' - jk''$, we obtain:

$$\{1 - \omega_0^2/\omega^2 - j/Q\} + \kappa \{\cos(k'a) \cosh(k''a) + j \sin(k'a) \sinh(k''a)\} = 0 \tag{3}$$

Here, $\omega_0 = 2\pi f_0 = 1/\sqrt{(LC)}$ is the angular resonant frequency of each element, and f_0 is the corresponding temporal frequency. Equation 3 may be solved exactly for given ω, Q and κ, to find k'a and k''a. Equating real and imaginary parts separately to zero, we obtain:

$$\begin{aligned} (1 - \omega_0^2/\omega^2) + \kappa \cos(k'a) \cosh(k''a) &= 0 \\ - 1/Q + \kappa \sin(k'a) \sinh(k''a) &= 0 \end{aligned} \tag{4}$$

If the losses are small, $k''a << 1$ and we may find an approximate solution in the form:

$$\begin{aligned} (1 - \omega_0^2/\omega^2) + \kappa \cos(k'a) &= 0 \\ k''a &= 1/\{\kappa Q \sin(k'a)\} \end{aligned} \tag{5}$$

The upper equation in (5) is the dispersion relation for lossless MI waves. Propagation is obtained only over the frequency band $1/(1 + \kappa) \le (\omega/\omega_0)^2 \le 1/(1 - \kappa)$, whose extent

depends on the value of κ, and hence on the strength of the mutual inductance between the loops. Figure 2a shows the dispersion characteristic for two different values of κ. In each case, the exact solution (Equation 4) is compared with the approximate solution (Equation 5). In the lossless case, $ka \rightarrow 0$ at the low-frequency limit, while $ka \rightarrow \pi$ at the high-frequency limit. At the band centre, when $\omega \approx \omega_0$, $ka \approx \pi/2$. Differences between the exact and the approximate solution occur at the band edges, and the effect of loss is to allow propagation outside the ideal band. For $\kappa = 0.25$, the band is larger than for $\kappa = 0.125$.

The lower equation in (5) gives the approximate variation of loss. Losses are inversely proportional to Q, as might be expected. However, they are also inversely dependent on κ, so that low loss is only obtained using strongly coupled chains of high Q resonators. Figure 2b shows the frequency variation of loss, for the same two values of κ as Figure 2a, assuming that $Q = 50$. Again, exact and approximate results are shown, and differences between the two occur at the band edges. Lower loss is obtained when the coupling is stronger. Loss is minimised at midband, and the minimum loss is $k''a_{min} \approx 1/\kappa Q$. Using Equation 5, minimum losses can be estimated for different lines as shown in Table I. Clearly, high coupling coefficients and Q factors will be required in practical devices.

κ	Q	Minimum k''a	Minimum loss per section (dB)
0.125	50	0.160	0.695
0.250	50	0.080	0.347
0.125	100	0.080	0.347
0.250	100	0.040	0.174
0.125	200	0.040	0.174
0.250	200	0.020	0.087

Table I. Estimated minimum propagation losses for different magnetoinductive waveguides.

2.2 *Dispersion characteristic for second-nearest neighbour coupling*

If the coupling is strong, modifications may be needed to the above theory. Particularly, if second-nearest neighbour coupling is included, the governing equation becomes:

$$(1 - \omega_0^2/\omega^2 - j/Q) + \kappa_1 \cos(ka) + \kappa_2 \cos(2ka) = 0 \tag{6}$$

Here, $\kappa_1 = 2M_1/L$ is the coupling coefficient and M_1 is the mutual inductance for nearest neighbours, and $\kappa_2 = 2M_2/L$ and M_2 are the corresponding values for second-nearest neighbours. The equations that must be solved for the real and imaginary values of the propagation constant now become:

$$\begin{aligned}(1 - \omega_0^2/\omega^2) + \kappa_1 \{\cos(k'a)\cosh(k''a) + \xi_2 \cos(2k'a)\cosh(2k''a)\} = 0 \\ - 1/Q + \kappa_1 \{\sin(k'a)\sinh(k''a) + \xi_2 \sin(2k'a)\sinh(2k''a)\} = 0\end{aligned} \tag{7}$$

Here the normalised parameter $\xi_2 = \kappa_2/\kappa_1$ represents the strength of the second neighbour interaction. In the low loss regime, Equations 7 may be approximated as before by:

$$\begin{aligned}(1 - \omega_0^2/\omega^2) + \kappa_1 \{\cos(k'a) + \xi_2 \cos(2k'a)\} = 0 \\ k''a = 1/\{\kappa_1 Q\,[\sin(k'a) + \xi_2 \sin(2k'a)]\}\end{aligned} \tag{8}$$

Figure 3a shows dispersion characteristics obtained from Equation 8 for $\kappa_1 = 0.25$ and $Q = 50$, i) for nearest neighbour interactions only, and ii) first and second neighbour interactions, with $\xi_2 = 0.25$. In the former case, the dispersion characteristic is much as before. However, in the latter, the characteristic is shifted down in frequency, and flattened at high frequencies. In fact, we have shown elsewhere [5] that the dispersion characteristic no longer increases

monotonically for $\xi_2 > 0.25$, so there is the possibility of a second propagating wave at some frequencies. Under other conditions, two waves are still supported, although the second wave is a rapidly attenuated evanescent type. Figure 3b shows the corresponding loss variations. Clearly, both these characteristics could be computed using the more accurate Equation 7, and further modifications would be expected near the band edges.

2.3 Dispersion characteristic for generalised non-nearest neighbour coupling

In general, coupling between each element and an arbitrary number of neighbours may be significant. The number that must be taken into acount is determined by the rate at which mutual inductance varies with element separation. Mutual inductance is difficult to model for many real inductors, and standard expressions exist only for simple cases (such as a large circular coil coupled to a smaller coil placed on-axis). However, experimentally, it is simple to determine the mutual inductance M(a) as a function of the element separation a. Once this variation is known, the coupling terms may be estimated using simple functions.

For example, over a reasonable range, the mutual inductance of real in ductors often varies as an inverse power of separation, so we may write $M(a) = M_0 a^{-p}$. This approximation is unsuitable for small a; the mutual inductance must peak at $\pm L$, so that $|\kappa_1| \leq 2$. However, within the range of validity of the approximation, $M_2/M_1 = 2^{-p}$, $M_3/M_1 = 3^{-p}$, and so on. In the low-loss case, we then obtain the following simple estimates for dispersion and loss:

$$(1 - \omega_0^2/\omega^2) + \kappa_1 \sum_{i=1}^{N} \xi_i \cos(ik'a) = 0$$

$$k''a = 1/\{\kappa_1 Q [\sum_{i=1}^{N} \xi_i \sin(ik'a)]\} \qquad (9)$$

Here the normalised coupling ratios ξ_i are $\xi_i = \kappa_i/\kappa_1 = i^{-p}$. For a square law decay of mutual inductance, $\xi_2 = 1/4 = 0.25$ (as in the previous sub-section), $\xi_3 = 1/9$, $\xi_4 = 1/16$ and so on.

Figure 3 shows dispersion and loss characteristics for this case, assuming all possible interactions. There are clearly further significant modifications to the results.

2.4 Experimental aims

With this background, a number of key aims for initial experiments may be identified:

- To develop a simple method of constructing well-matched, high Q resonators
- To develop a simple test bed for arranging the resonators in a waveguide geometry
- To investigate the variation with element separation of the coupling coefficient κ
- To demonstrate propagation of magnetoinductive waves with different values of κ and Q
- To develop methods for determining the dispersion and loss characteristics
- To establish the relative significance of non-nearest neighbour coupling
- To investigate the prospects for quasi-optical devices based on MI waveguides

3. Low frequency experiments

We now describe the results of initial experiments performed at low frequency. Resonant elements were constructed using printed circuit board (PCB) elements and external capacitors. The PCBs were designed for insertion into grooved nylon baseboards to form magneto-inductive waveguides in the forward wave configuration.

3.1 Resonant elements

The PCBs carried square spiral inductors in Cu on FR-4, with the layout shown in Figure 4a. Devices with different numbers of turns were fabricated. Their impedance was measured using an Agilent E5061A ENA Series Network Analyser, which was purchased for the project, and a pair of simple needle probes. Inductance data measured at 10 MHz is shown in Figure 4b. The inductance does not scale with the square of the number of turns (as would be expected from elementary theory) because of the finite conductor width, which diminishes the enclosed area significantly. Measured reactance data for multiple turn devices is shown in Figure 4c. There is a measurement system artefact caused by the probes at 100 MHz, which should be ignored. The rise in reactance at high frequency is caused by self-resonance arising from the capacitance between the inductor winding and the air-bridge. The self-resonant frequency is rather low (ca 415 MHz) for five turn inductors. Three turn inductors were selected as being most suitable for further experiments, because they have reasonably large inductance (ca 140 nH) and a high self-resonance (ca 560 MHz).

Low-frequency L-C resonators were constructed using the PCB inductors and 0805-type SMD capacitors. Figure 5a shows the frequency variation of the complex impedance $Z = R + jX$ for a resonator formed from a three-turn inductor and a 100 pF capacitor. The resonant frequency is $f_0 \approx 41.87$ MHz. The quality-factor was determined from the width of

the impedance bandpass as $Q \approx 50$. A typical variation of $|Z| = \sqrt{(R^2 + X^2)}$ used in Q-factor determination is shown in Figure 5b.

Resonators were formed in batches in a similar way. Considerable scatter in resonant frequency was observed, arising from the relatively poor tolerance of the surface mount capacitor value. For example, Figure 6a shows the frequency variation of R for a set of un-tuned elements. Matching within fraction of pass-band was possible using additional shunt capacitors, although the matching process was extremely tedious. Figure 6b shows the frequency variation of R for a set of elements matched to $f_0 \approx 42$ MHz.

3.2 Coupling Coefficient

Factors affecting the coupling coefficient κ were investigated first, using the arrangement shown in Figure 7a. Two resonant elements were inserted into a baseboard at a defined relative position. The coupled resonator system was excited using a weak inductive probe and the scattering parameter S_{11} was measured. Typically, two resonances were observed, as shown in Figure 7b. These correspond to the symmetric and anti-symmetric modes of the two-element system, which have angular resonant frequencies $\omega_1 = 1/\sqrt{\{(L + M)C\}}$ and $\omega_2 = 1/\sqrt{\{(L - M)C\}}$. The corresponding frequencies f_1 and f_2 were then compared with the resonant frequency f_0 of an isolated element, allowing κ to be determined as:

$$\kappa = 2M/L = 2\{(f_0/f_1)^2 - 1\} = 2\{1 - (f_0/f_2)^2\} \tag{9}$$

Figures 8a and 8b show the experimental variation of f_1, f_2 and κ with axial element separation. The range of available data is limited. The minimum separation is limited by the thickness of the PCB and capacitor. The maximum separation is limited by the difficulty of accurately distinguishing two low-Q split resonances. Over the range shown, the variation

follows an inverse square law, to a reasonable approximation. A similar trend was obtained when the experiments were repeated using bare three-turn inductors (i.e. inductors without an additional capacitor) at their self-resonant frequency. However, there are departures from the inverse square law for small separations, since the mutual inductance must tend to a finite value as the separation tends to zero. This result implies that the coupling coefficient for second neighbours will generally be one quarter that of the coupling coefficient for nearest-neighbours, and that several non-nearest interactions will indeed be significant.

A similar experimental arrangement allowed the coupling coefficient κ' to be measured as a function of the lateral element offset. Figure 8c shows the experimental variation of the coupling ratio $\mu = \kappa'/\kappa$ with lateral element offset, for two values of axial separation. In each case, μ varies with offset in an approximately Gaussian manner. This result shows that μ is strongly affected by misalignments greater than around 1 mm, so that accurate lateral alignment of the elements forming a waveguide will be required for low scattering.

3.3 Magneto-inductive Waveguides

Magneto-inductive waveguides were constructed by inserting different numbers of elements into a grooved baseboard as shown in Figure 9a. To minimise scattering from line non-uniformities, each element's resonant frequency f_0 was re-measured, and the elements were inserted in order of increasing resonant frequency as shown in Figure 9b. Here, the majority of the elements lie within $\pm$ 0.25% of the average frequency.

A variety of input an output transducers were investigated, including directly-connected inductors, directly connected resonators, and resonators excited inductively by directly-connected and closely-spaced inductors. The latter were found consistently to give the lowest insertion loss and hence were used in subsequent experiments.

Short waveguides were assessed first, to show the gradual development of the magneto-inductive wave band. Figure 10 shows the variation of S_{11} and S_{21} with frequency for a) a one-element MI waveguide, and b) a two-element MI waveguide. The axial separation is 4 mm (corresponding to $\kappa \approx 0.25$). In the first case, a single resonance may be seen, and in the second, two split resonances. Figure 11 shows similar results for three- and four element waveguides, where the number of resonances has increased to three and four, respectively. As the number of resonances increases, the resonances move closer together. However, the resonances appear less pronounced as their frequency increases, suggesting that losses increase with frequency.

Longer waveguides were then assessed. For example, Figure 12a shows the frequency variation of S_{11} and S_{21} for a 30-element MI waveguide. The axial separation is again 4 mm. There are now no discernable separate resonances, and transmission clearly takes place across a band of frequencies. The relatively small reduction in S_{11} over this band implies that the coupling efficiency into the MI waveguide is relatively poor. Similarly, the low maximum value of S_{21} implies that the propagation losses are relatively high, and also increase rapidly near the band edges.

Figure 12b shows a comparison of S_{21} for MI waveguides with 3.5, 4, 5 and 7 mm axial element separation. In the last case, the waveguide was shortened to 25 elements, because of the increased losses. The smaller value of κ obtained with the wider element separation results in a reduction in the width of the MI band, and an increase in loss, as would be expected from the theoretical introduction. The "shoulder" appearing just beyond the high frequency cut-off off the MI wave seems to be characteristic, but, since the transmission is very low at this point, the measurement may not be reliable.

The dispersion characteristics were determined by measuring the phase delay $\arg(S_{21})$, and dividing by the number of elements N in the line. Unfortunately this measurement is inaccurate, due to the ambiguities of 2π in phase inherent in the method and the possibility of a non-monotonic variation. Initial data are shown in Figure 13a for a line with i) 3.5 mm, ii) 4 mm and iii) 5 mm axial separation. The data have been compared with the theoretical estimate for a low-loss line with Q = 50 and i) $\kappa_1 = 0.3$, ii) $\kappa_1 = 0.25$, and iii) $\kappa_1 = 0.17$, and assuming an inverse square decay of the mutual inductance. There is quite reasonable agreement, but the experimental data are clearly unreliable at high frequency. The agreement is much worse if non-nearest neighbour interactions are omitted from the model.

The frequency variation of the attenuation was then found by measuring S_{21} for lines with different element numbers N_1 and N_2, subtracting the two sets of data, and dividing the result by $\Delta N = N_1 - N_2$. Similar results were obtained for different ΔN, but oscillations due to Fabry-Perot effects were found for small ΔN. Figure 13b shows the variation of attenuation with frequency for MI waveguides with 4 mm element separation. The minimum loss is around 0.4 dB/section; this value is similar to the estimate in the Introduction. The attenuation clearly rises at the band edges. A theoretical comparison is again shown. The experimental losses are generally higher then the theoretical prediction, suggesting that the transmission has been reduced by back scattering in addition to absorption.

3.4 Interim conclusions

The experiments described above have shown that it is reasonably simple to construct magneto-inductive waveguides with modest performance, to determine their performance characteristics and to compare these with theories containing different levels of detail. A number of conclusions may be reached. To develop useful devices based on magneto-inductive waves, it will be important to increase throughput. The operation of input and

output transducers should therefore be studied, and insertion losses optimised. Propagation losses should also be reduced, by minimising scattering and increasing the Q-factor. To develop easily controllable devices, non-nearest neighbour interactions should also be suppressed. It is therefore important to investigate circumstances under which the coupling coefficient will decay more rapidly than with the inverse square of the element separation.

4. High frequency experiments

Experiments were therefore carried out with alternative resonant elements, with the aim of addressing all the points above.

4.1 Reduction of non-nearest neighbour coupling

To reduce the effects of non-nearest neighbour coupling, the following strategy was adopted. For planar coils, the situation is as shown in the upper diagram of Figure 14a. Nearest neighbours are separated by the element repeat distance, second neighbours by twice this value, and so on. Assuming that mutual inductance decays as an inverse power of separation, the ratio of the i^{th} higher coupling term to the fundamental is $\xi_i = \kappa_i/\kappa_1 = i^{-p}$, where we have shown that $p \approx 2$. For solenoidal coils, the situation is as shown in the lower diagram. Here the distance between the coil ends is a - L for nearest neighbours, 2a - L for second neighbours, and so on, where L is the coil length. The effect of a finite coil thickness is therefore to move nearest neighbours relatively closer to each other than higher ones. As a result, we would expect the coupling ratio to modify to $\xi_i = \kappa_i/\kappa_1 = \{(i - L/a) / (1 - L/a)\}^{-p}$. Table I shows how the first few coupling ratios might be expected to modify, assuming p = 2. Significant reductions in ξ_2 occur – for example, over 50% for L/a = 0.5.

L/a	ξ_2	ξ_3	ξ_4
0	0.2500	0.1111	0.0625
0.25	0.1836	0.0744	0.0400
0.50	0.1111	0.0400	0.0204
0.75	0.0400	0.0123	0.0059

Table II. Estimated coupling ratios for "solenoidal coils" of different fractional lengths.

To implement this idea in practise, elementary "solenoidal" coils were constructed by modifying the previous PCBs to incorporate windings on both sides as shown in Figure 14b. To begin with, three-turn coils were configured as resonators at ca 150 MHz frequency using additional capacitors and the coupling coefficient was measured as a function of the element repeat distance as described before.

Figure15 a shows the result. The variation for "solenoidal" coils is almost exactly the same as that for planar coils, when the latter are shifted closer together by the PCB thickness. This result essentially validates the assumptions above. The data were then used to estimate the value of the coupling ratio $\xi_2 = \kappa_2/\kappa_1$, as shown in Figure 15b. The value of ξ_2 is not exactly 0.25 for planar coils, as implied by a simple power law decay of mutual inductance. Instead, it ranges from around 0.1 (for weakly coupled elements) to 0.5 (for strongly coupled ones). However, the solenoidal coils do indeed show a significant reduction in the second neighbour coupling ratio, by almost 50% over the range assessed. Solenoidal coils were therefore used for subsequent experiments.

4.2 Magneto-inductive waveguides based on self-resonant elements

To increase the operating frequency, and perhaps more importantly to eliminate the need for an external capacitor, coils were operated in a self-resonant mode. Unfortunately, three-turn, "solenoidal" coils had a very high resonant frequency (> 300 MHz), and hence appeared very sensitive to parasitic capacitances and other external disturbances. The bulk of the remaining work was therefore carried out using five-turn "solenoidal" coils, which resonated at around 200 MHz frequency, and which appeared more stable. Their coupling characteristics were very similar.

Figure 16a shows the variation of resonant frequency with element number, for a batch of

100 self-resonant elements based on five-turn "solenoidal" coils. The resonant frequency is now $f_0 \approx 205.25$ MHz, and around 60% of the elements have resonances lying within ± 0.2% of f_0. Figure 16b shows the same data plotted as a distribution, showing the essential Gaussian nature of the statistics. This result should be compared with Figure 9b, where a similar frequency spread was achieved only after laborious frequency matching.

Magneto-inductive waveguides were constructed using elements taken from the central region of this distribution. Figure 17 shows a) the frequency variation of S_{21} and b) the dispersion characteristics for 30 element waveguides, with different axial element spacing. The overall insertion loss has clearly now reduced below 10 dB for the most strongly coupled line (with a = 3 mm), and the dispersion characteristic now more closely resembles the ideal obtained with only nearest-neighbour coupling. Even longer lines were constructed from these elements. For example, Figure 18 shows the variation of a) S_{21} and b) S_{11} with frequency for MI waveguides with 3 mm element spacing and up to 60 elements. From Figure 18a, the losses at mid-band can be seen to have reduced below 0.3 dB per element, and it is likely that losses could be reduced still further by optimising the coil Q-factor.

4.3 Optimisation of input and output coupling

The apparent performance of a magneto-inductive waveguide is strongly affected by the input and output coupling loss in addition to propagation loss. At the start of the project, this aspect was not fully understood, and coupling was optimised heuristically. As has been mentioned, the transducers giving the best performance were closely spaced inductors, connected to the ENA by a short section of 50 Ω line. By the end of the project, this aspect was understood, and we now give a brief explanation.

In earlier theoretical work [1, 6], it was shown that an abruptly terminated line could have

zero reflection when additional impedance Z_T was inserted into the final element. If the termination is at element n, element n + 1 is absent, and Equation 1 modifies to:

$$\{R + j\omega L + 1/j\omega C + Z_T\}I_n + j\omega M\{I_{n-1}\} = 0 \quad (10)$$

Assuming a current wave $I_n = I_0 \exp(-jk_n a)$ is incident, comparison between Equations 1 and 10 shows that there will be no reflection if $Z_T I_n = j\omega M I_{n+1}$, i.e. if $Z_T = j\omega M \exp(-jka)$. Because this value of Z_T represents the line impedance, a key consequence is that (in contrast to a coaxial guide) the impedance of a MI waveguide is neither real nor constant, being strongly affected both by the mutual inductance M and by the frequency ω. The task of providing a reflectionless termination is thus non-trivial, especially if the MI waveguide must in addition be connected to a line of fixed impedance.

In [1], it was shown that the problem was simplified if only a single frequency need be considered. For example, at mid-band, when $ka = \pi/2$, Z_T has the (real) value ωM. Insertion of a resistor of this value into the final element would therefore provide a reflectionless termination at mid-band, with increasing return loss towards the band edges. Unfortunately, while an ENA has real impedance, it does not necessarily have the correct impedance even to provide this limited degree of matching. Thus, simply connecting the ENA to the first and last elements in a MI waveguide does not provide a satisfactory solution.

In our experiments, the best results were obtained by directly connecting the ENA to planar coils of a given number of turns, and then inductively coupling the coils to the first and last elements of the MI waveguide as shown in Figure 18a. Here, M' is the mutual inductance between the final element and the transducer, which has inductance L'. Clearly, the effect of this arrangement is to insert an impedance Z in the last element whose value is effectively

that of the ENA scaled by the turns-ratio of the resulting transformer. Crucially, varying the turns-ratio allows the matching to be optimized for lines with different values of ω or M.

For example, Figure 18 shows the frequency variation of b) S_{11} and c) S_{21}, for magneto-inductive waveguides based on five-turn self-resonant "solenoidal coils", with an axial spacing of 3 mm and with input and output transducers based on planar coils with different numbers of turns. Clearly, the coupling is optimised for two-turn transducers, when S_{11} is minimised at midband and S_{21} is maximised. Even though the matching is effectively single-frequency, the oscillations in S_{21} (which are caused by multiple internal reflections) are significantly reduced across the band. Generally, matching proceeded by trial and error, adjusting the turns-ratio for a particular MI waveguide to obtain satisfactory performance.

4.4 Signal processing with MI waves

A variety of quasi-optical MI waveguide devices were proposed theoretically in [7]. The discovery of a matching method allowed the simplest (Fabry-Perot filters) to be constructed, without the effects of multiple reflections masking the device response. Filters were formed from otherwise uniform lines by adding a number of elements N to the line beyond the termination, allowing a cavity to be set up between the termination and the final element (as shown in Figure 19a for a cavity with N = 1). Figure 19b shows the frequency variation of S_{21} for a Fabry-Perot cavity with N = 1. Comparison with the response of a uniform line shows that the effect of the cavity is to insert a single notch, around 14 dB deep, at the centre of the MI band. Clearly, this notch is caused by interference between the signal at the termination and the reflection from the final element, which are in antiphase at midband (when $ka = \pi/2$). Figure 19c shows similar results obtained for a cavity with N = 2. There are now two notches, at frequencies when $ka = \pi/3$ and $ka = 2\pi/3$. Although embryonic, these results represent the first demonstration of signal processing with MI waves.

5. Conclusions

In this short investigative project, several important goals have been reached. These include:

- Development of high-performance resonant elements based on planar PCB structures
- Development of methods of controlling the coupling between elements
- Demonstration of low loss magneto-inductive waveguides over a range of frequencies
- Development of methods for matching to conventional waveguides
- Demonstration of elementary signal processing based on magneto-inductive waves

The waveguides perform well, and appear to behave in line with the predictions of simple theory based on equivalent circuits. The way therefore appears open to further investigation and exploitation of this interesting phenomenon. Possible applications include:

- Compact delay line filters (based on the slow speed of MI waves compared with EM waves)
- Systems for surface and subsurface detection (based on the sensitivity of an MI wave to an external perturbation of the magnetic field)
- Components for near-field control of RF signals (for example, guidance of detected RF signals in magnetic resonance imaging and spectroscopy)

6. Acknowledgements

The Authors are grateful to the USAF for sponsorship via EOARD, and to Lieut.-Colonel Michael Milligan for his continued support and encouragement.

7. References

1. Shamonina E., Kalinin V.A., Ringhofer K.H., Solymar L. "Magneto-inductive waveguide" Elect. Lett. 38, 371-373 (2002)
2. Shamonina E., Kalinin V.A., Ringhofer K.H., Solymar L. "Magnetoinductive waves in one, two and three dimensions" J. Appl. Phys. 92, 6252-6261 (2002)
3. Wiltshire M.C.K., Shamonina E., Young I.R., Solymar L. "Dispersion characteristics of magneto-inductive waves: comparison between theory and experiment" Elect. Lett. 39, 215-217 (2003)
4. Shamonina E., Solymar L. "Magneto-inductive waves supported by metamaterial elements: components for a one-dimensional waveguide" J. Phys. D. 37, 362-367 (2004)
5. Syms R.R.A., Shamonina E., Solymar L. "Magneto-inductive waveguides with second nearest neighbour interactions" unpublished manuscript
6. Syms R.R.A., Solymar L., Shamonina E. "Absorbing terminations for magneto-inductive waveguides" IEE Proc. Micr. Antennas Propag. 152, 77-81 (2005)
7. Syms R.R.A., Shamonina E., Solymar L. "Magneto-inductive waveguide devices" IEE Proc. Micr. Antennas Propag., accepted for publication

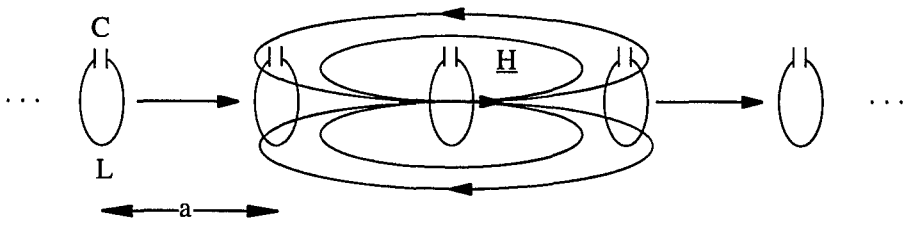

a)

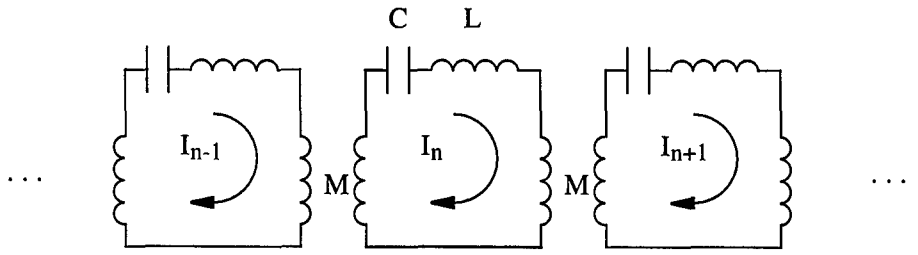

b)

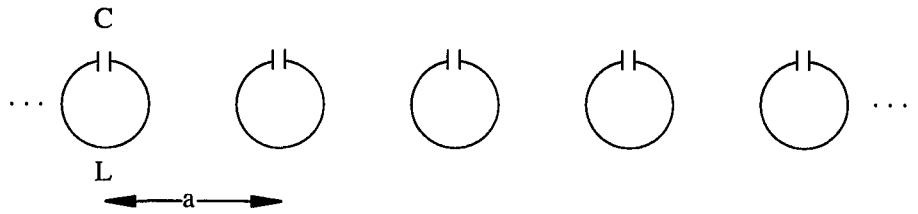

c)

Figure 1. a) Axial configuration for a magneto-inductive waveguide; b) equivalent circuit; c) the corresponding planar configuration.

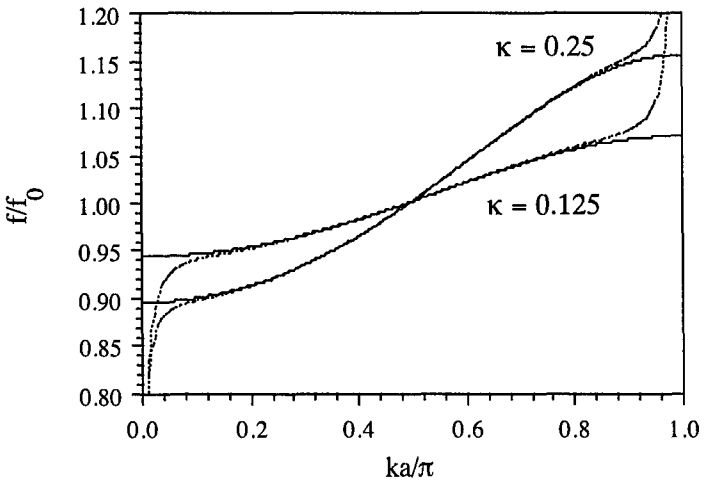

a)

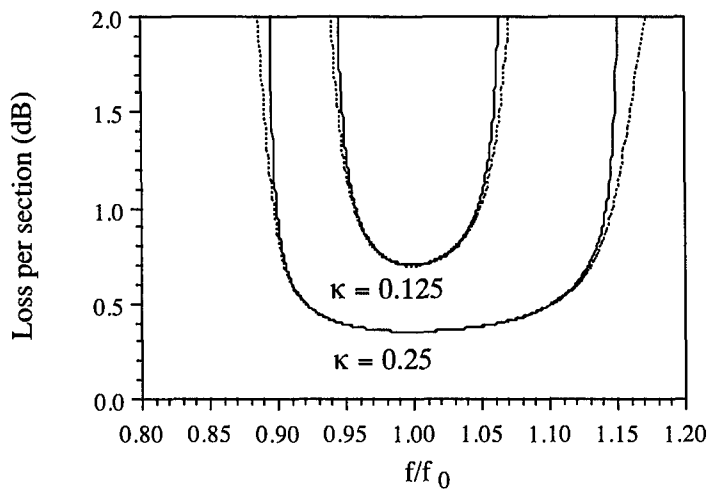

b)

Figure 2. a) Theoretical dispersion characteristic and b) frequency dependence of losses, for MI waveguides with Q = 50 and different values of κ. In each case, the full lines are approximate theory and the dotted lines are exact.

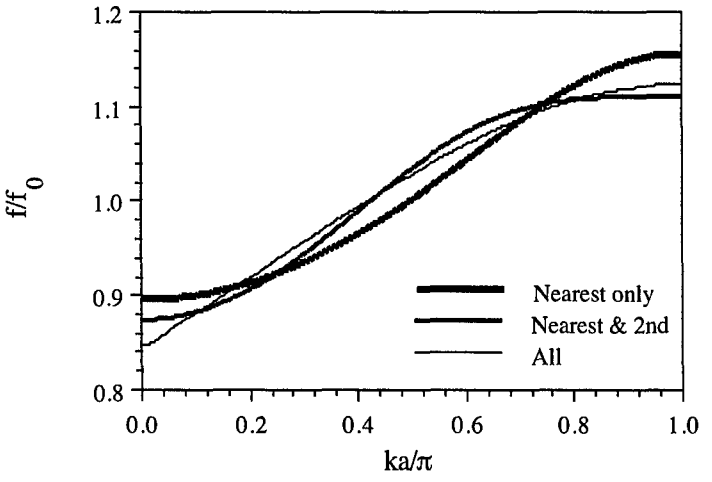

a)

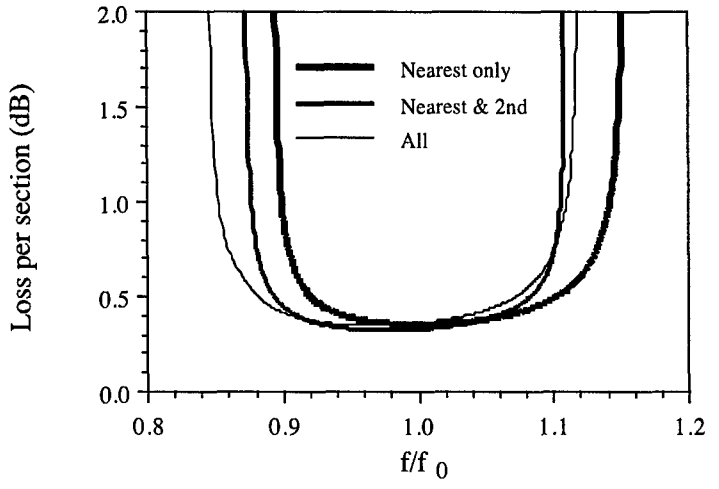

b)

Figure 3. a) Approximate theoretical dispersion characteristic and b) frequency dependence of losses, for MI waveguides with Q = 50 and $\kappa_1 = 0.25$, including i) only nearest neighbour interactions, ii) nearest and second nearest interactions, and iii) all interactions.

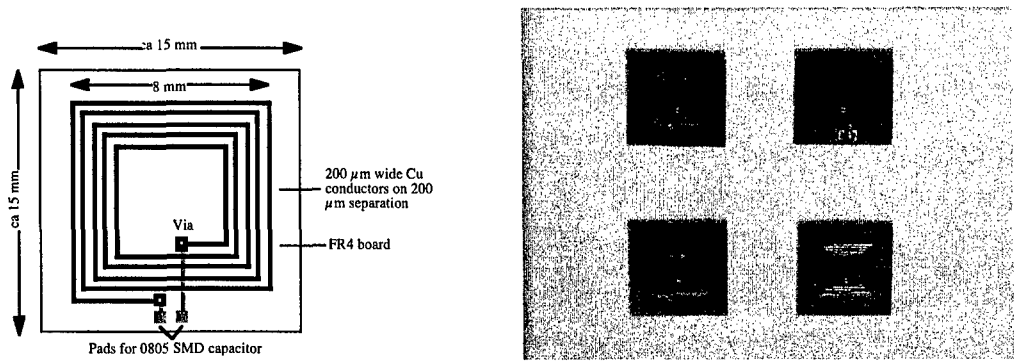

a)

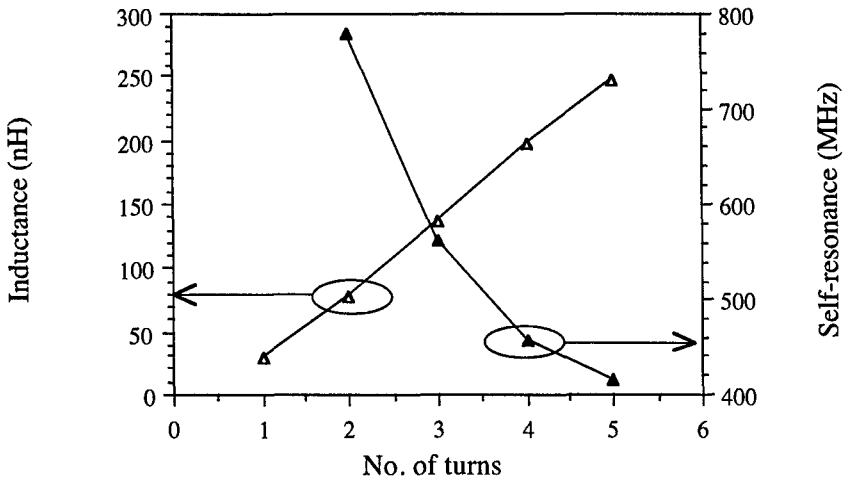

b)

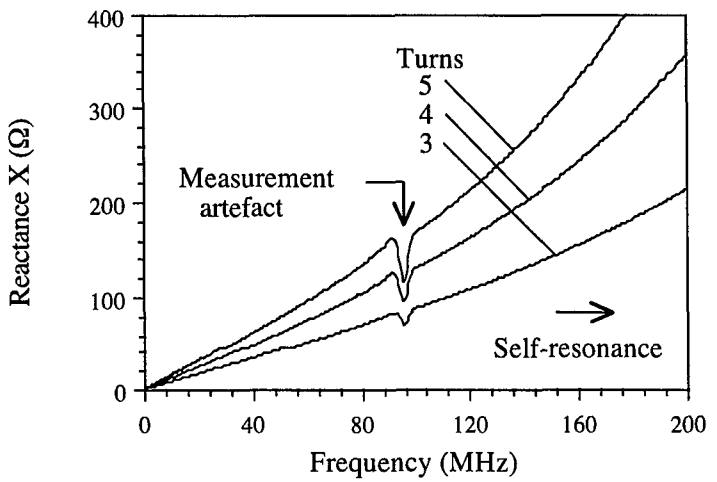

c)

Figure 4. a) Layout of different experimental inductors, b) variation of the inductor parameters with the number of turns, and c) variation of the reactance with frequency.

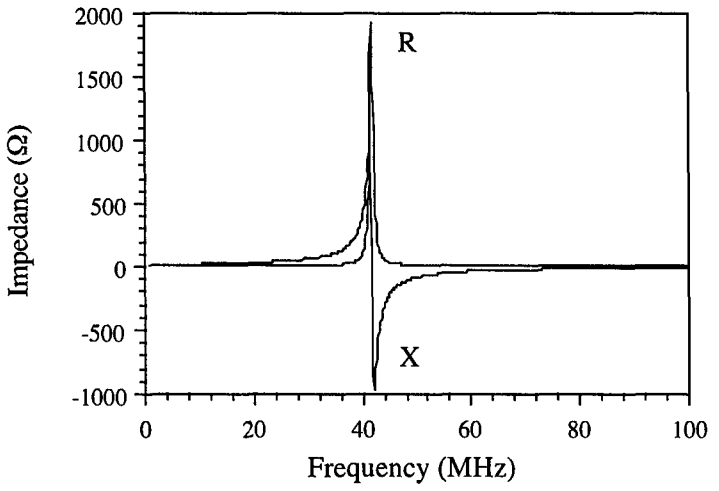

a)

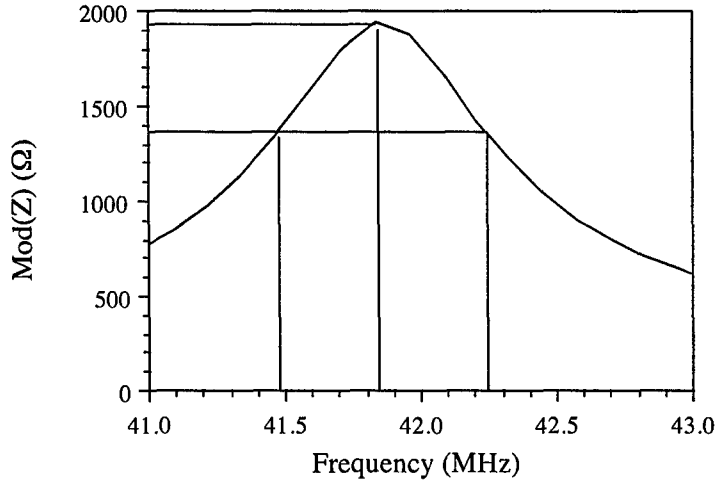

b)

Figure 5. Frequency variation of a) the complex impedance and b) the impedance modulus for a tuned element.

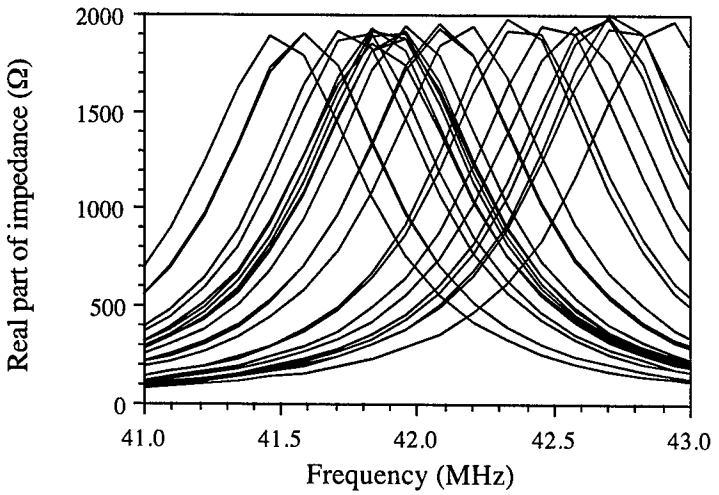

a)

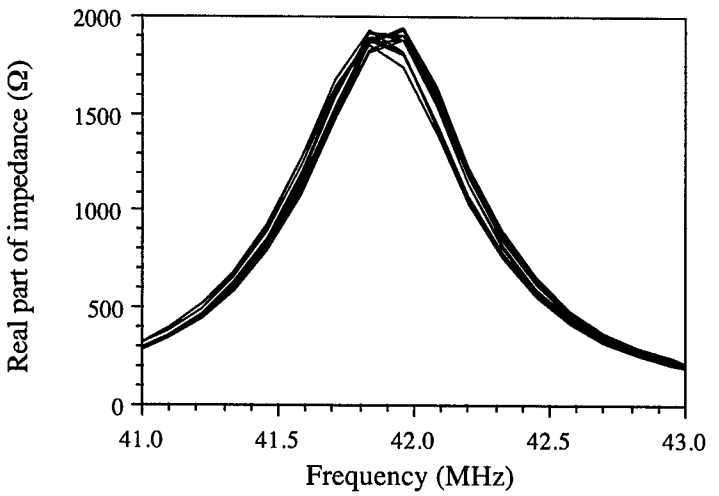

b)

Figure 6. Variation of real impedance for elements a) before and b) after matching.

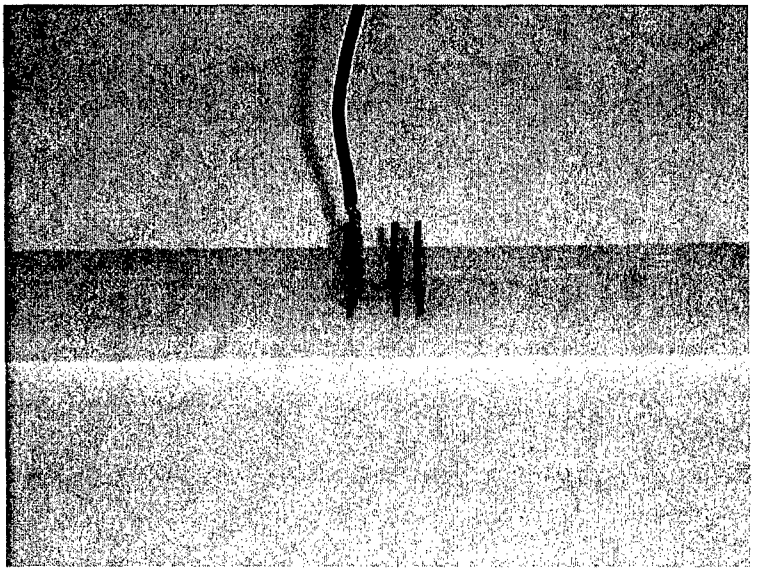

a)

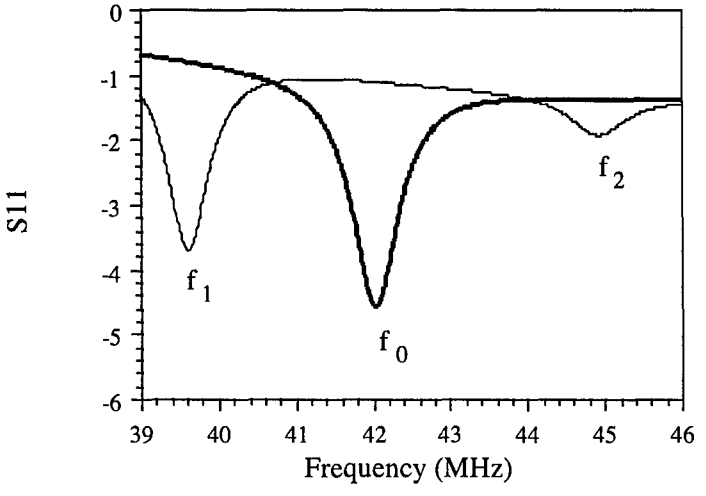

b)

Figure 7. a) Arrangement for inductive excitation of elements and b) resonant frequencies for single (thick line) and coupled (thin line) elements.

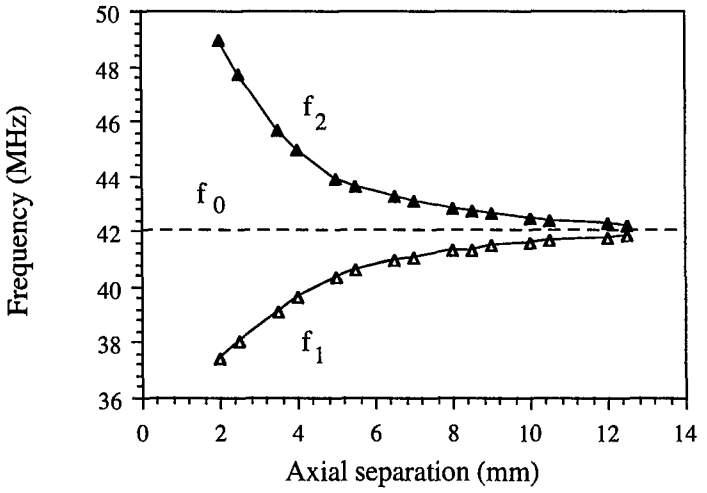
Frequency (MHz)
50
48
46
44
42
40
38
36
f_2
f_0
f_1
0
2
4
6
8
10
12
14
Axial separation (mm)

a)

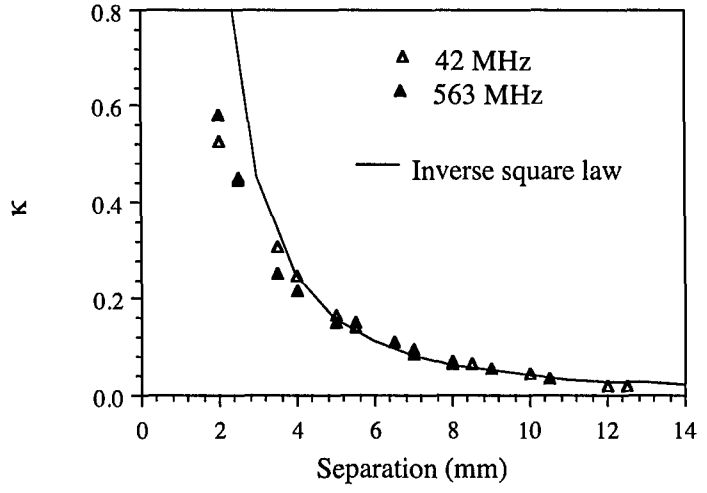
κ
0.8
0.6
0.4
0.2
0.0
42 MHz
563 MHz
Inverse square law
0
2
4
6
8
10
12
14
Separation (mm)

b)

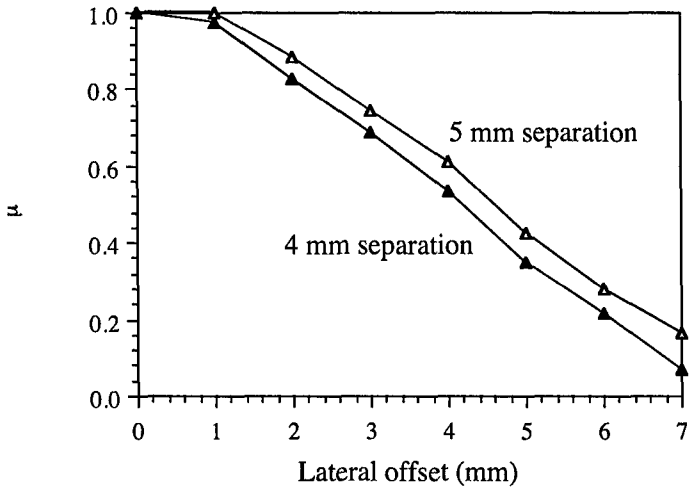

c)

Figure 8. Variation of a) resonant frequencies f_1 and f_2 and b) coupling coefficient κ with axial element separation a, and c) variation of the coupling ratio μ with lateral offset.

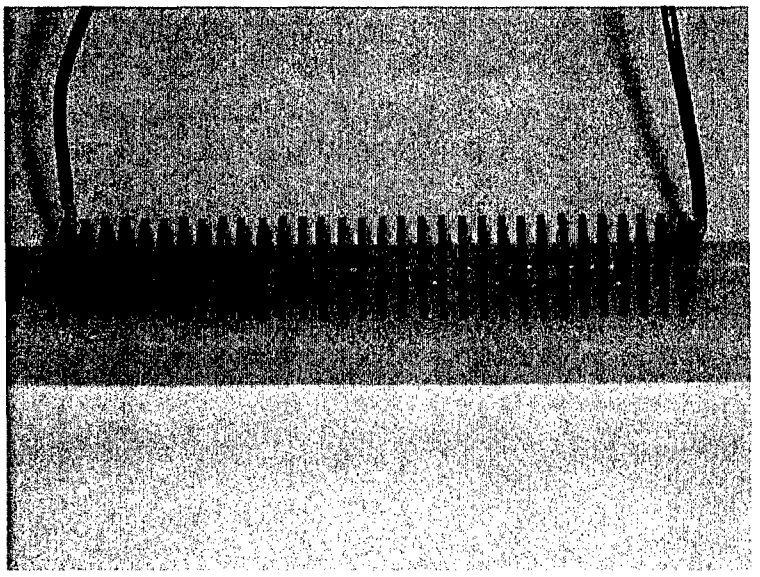

a)

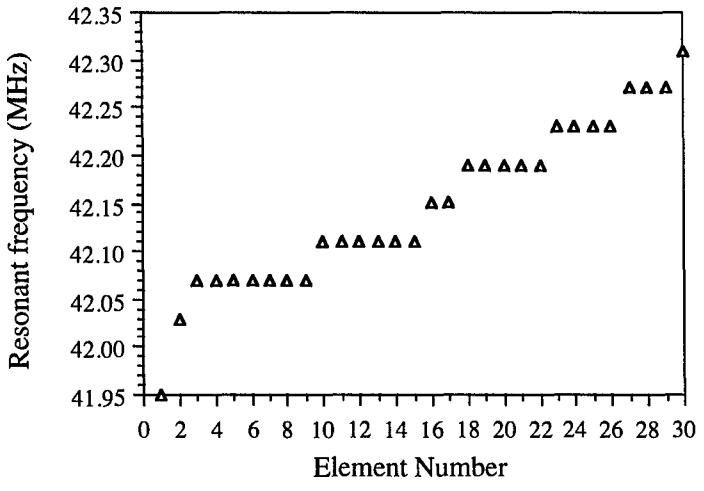

b)

Figure 9. a) Experimental MI waveguide, and b) resonant frequencies f_0 in an ordered 30-element line.

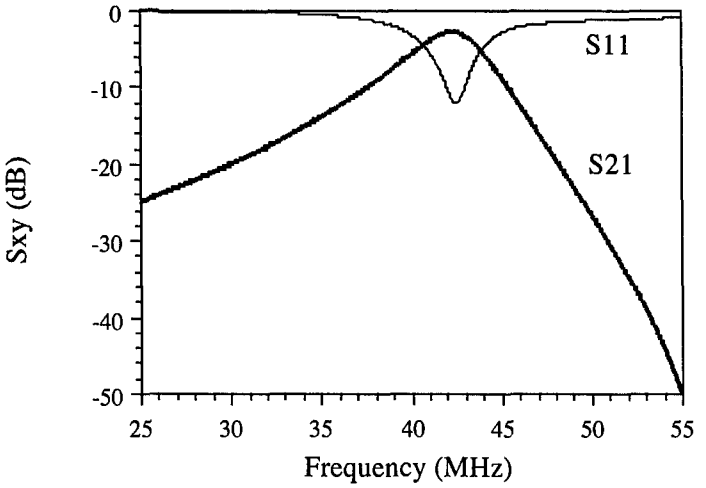

a)

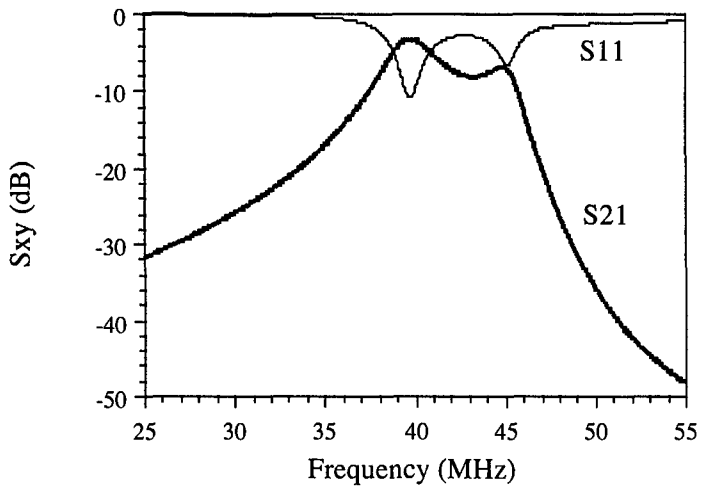

b)

Figure 10. Variation of S_{11} and S_{12} with frequency for a) a one-element and b) a two-element MI waveguide. The axial separation is a = 4 mm.

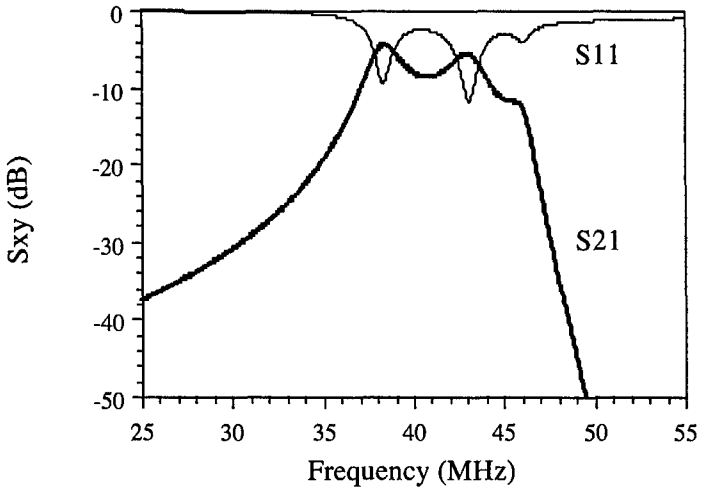

a)

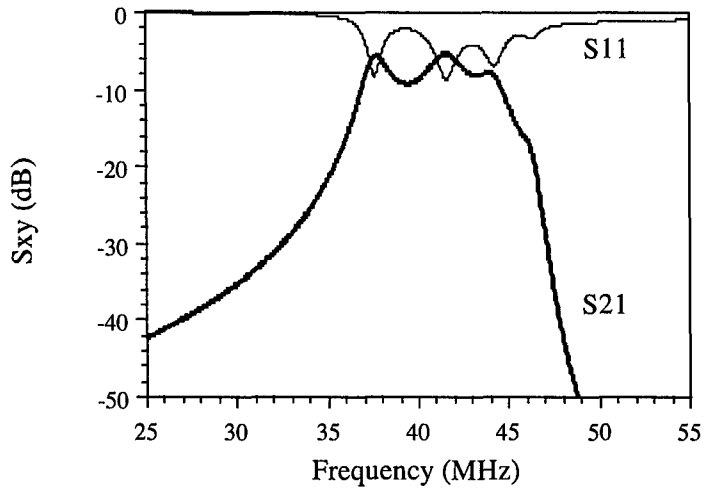

b)

Figure 11. Variation of S_{11} and S_{12} with frequency for a) a three-element and b) a four-element MI waveguide. The axial separation is a = 4 mm.

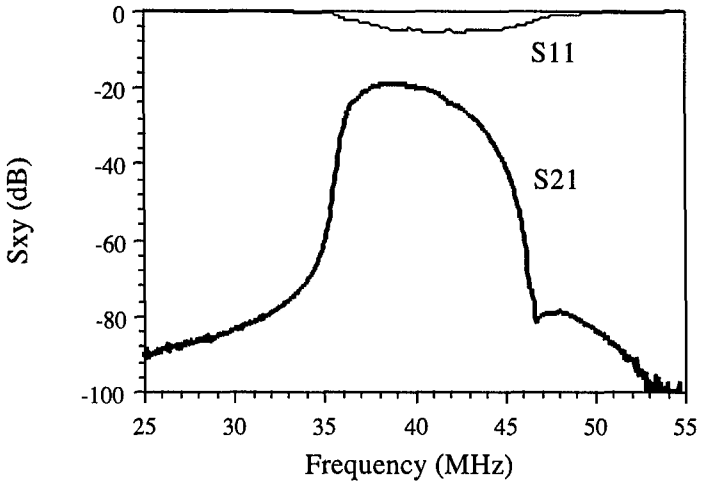

a)

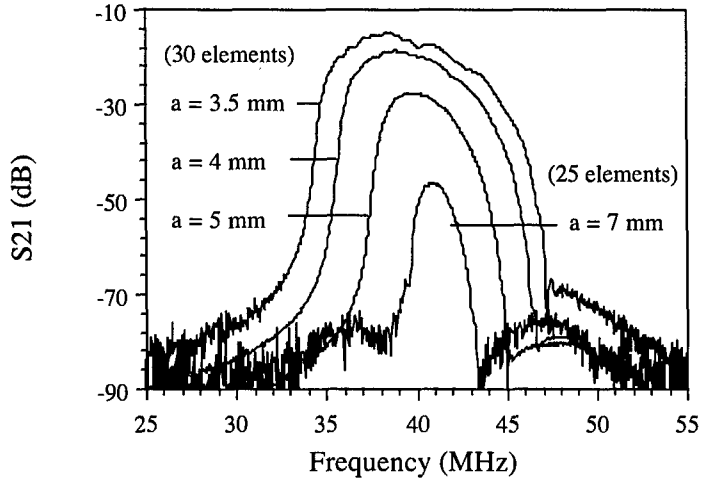

b)

Figure 12. a) Frequency variation of S_{11} and S_{21} for a 30-element MI waveguide with 4 mm axial element separation, and b) comparison of S_{21} for guides with different separations.

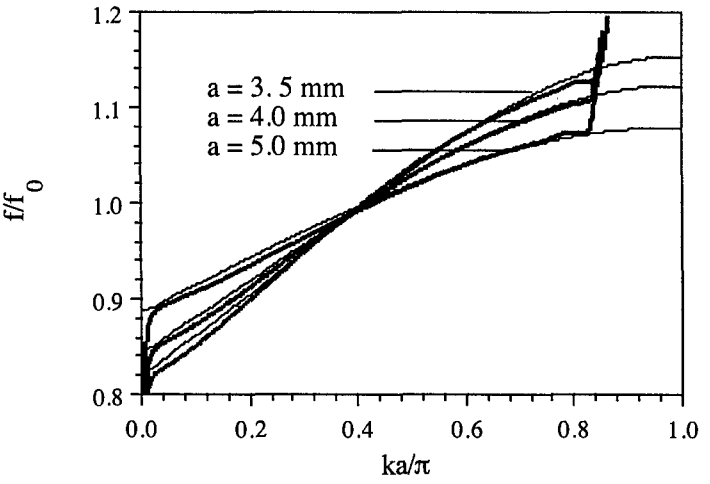

a)

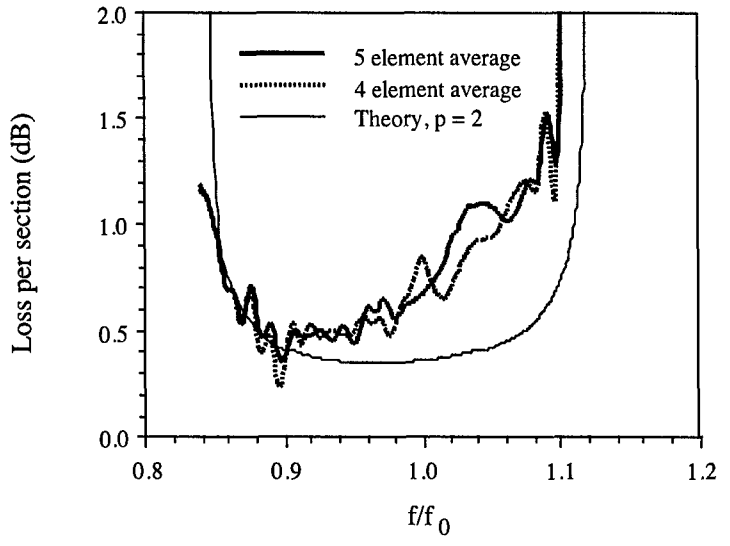

b)

Figure 13. a) Dispersion characteristic, and b) variation of attenuation with frequency, for MI waveguides with 4 mm axial element separation. The thick lines are experimental data, and the thin lines are predictions of theory.

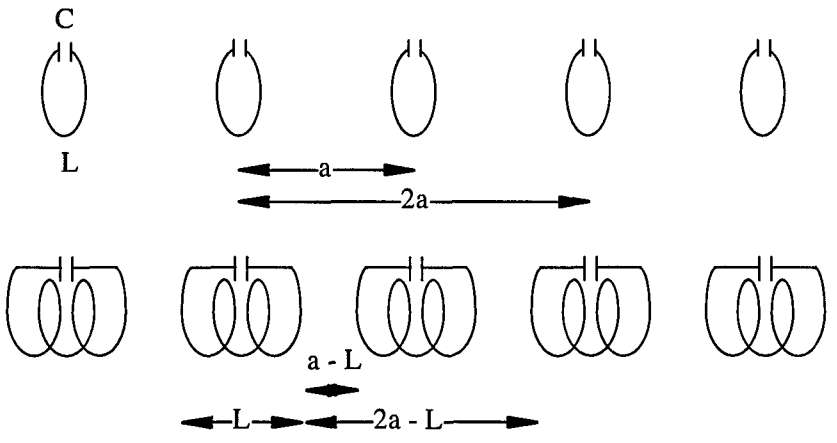

a)

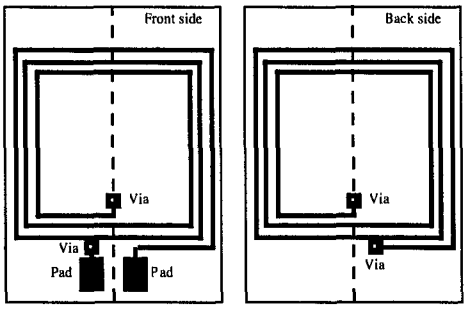

b)

Figure 14. a) MI waveguides based on planar and solenoidal coils; b) layout of "solenoids" based on double-layer PCBs.

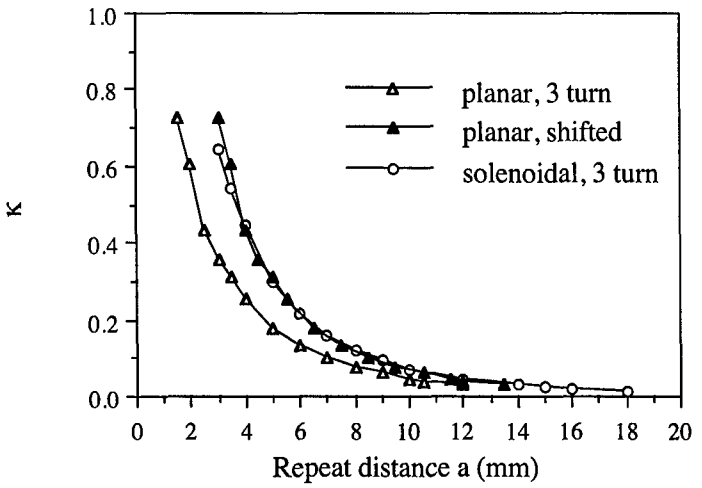

a)

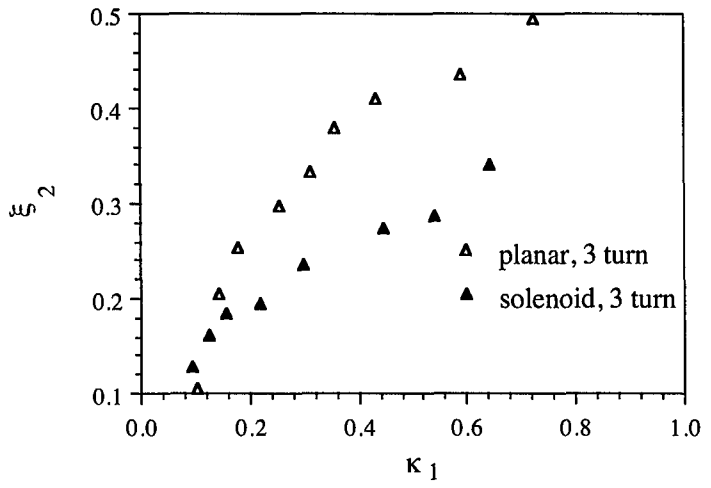

b)

Figure 15. a) Variation of κ_1 with a, and b) ξ_2 with κ_1 for planar and "solenoidal" coils

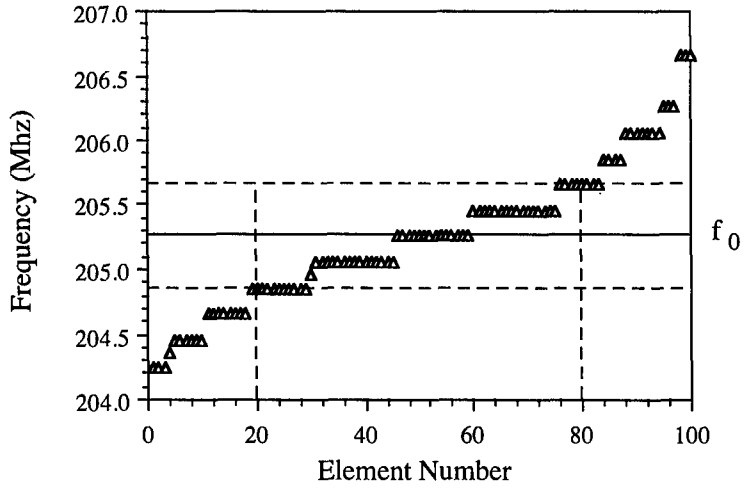

a)

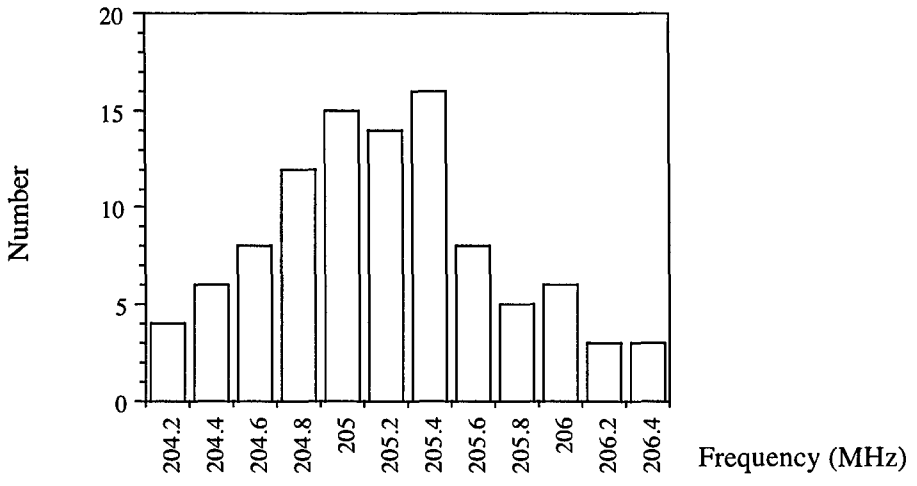

b)

Figure 16. a) Overall, and b) statistical variation of resonant frequency for a batch of 100 five-turn self-resonant "solenoidal" coils.

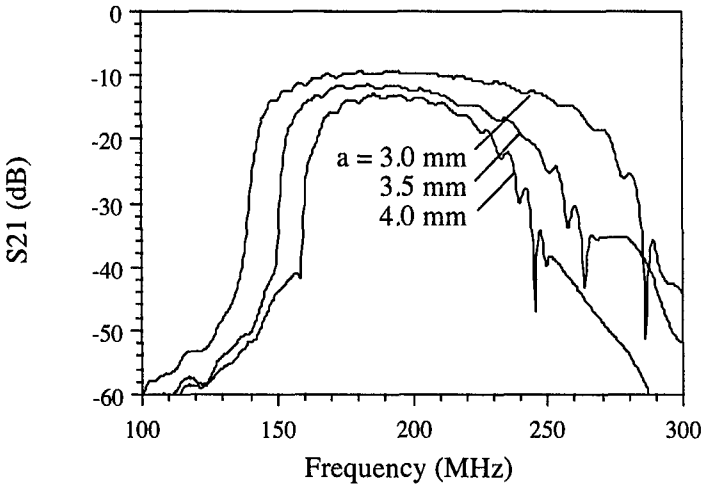

a)

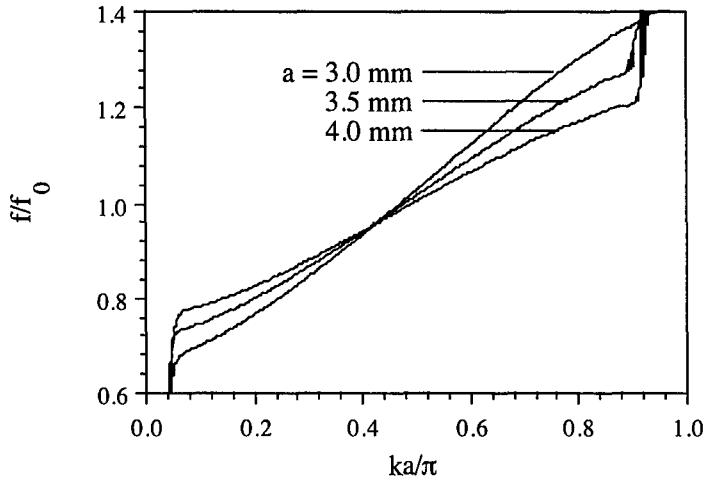

b)

Figure 17. a) Frequency variation of S_{21} and b) dispersion characteristics, for 30 element MI waveguides based on five-turn self-resonant "solenoidal" coils with different element spacings.

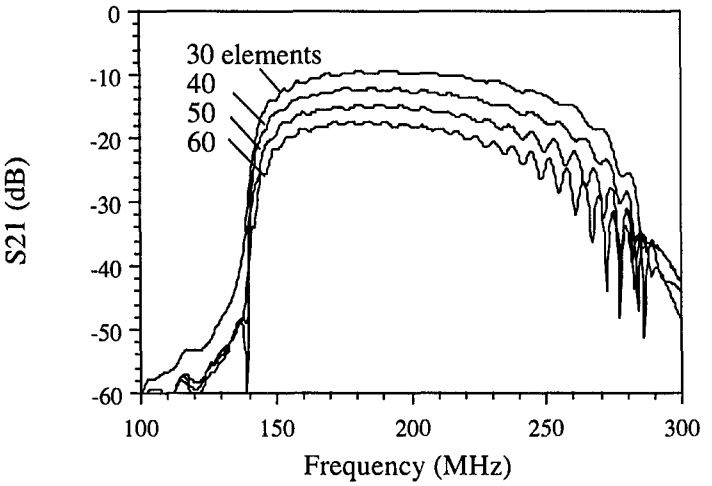

a)

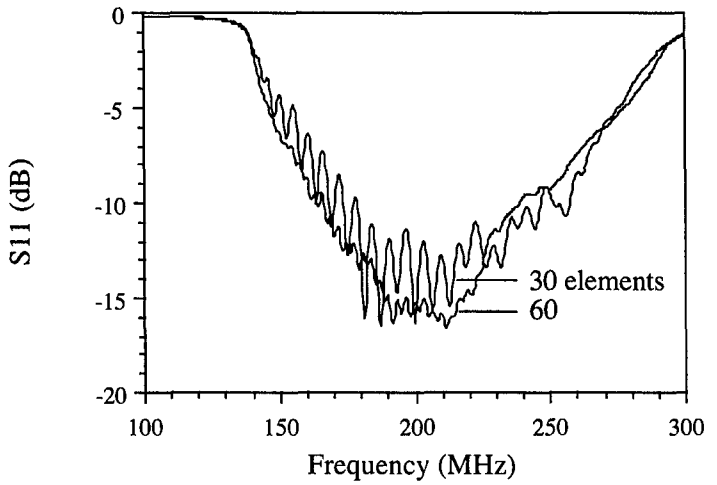

b)

Figure 18. Variation of a) S_{21} and b) S_{11} with frequency for MI waveguides with different numbers of elements, based on five-turn self-resonant "solenoidal" coils with 3 mm axial element spacing

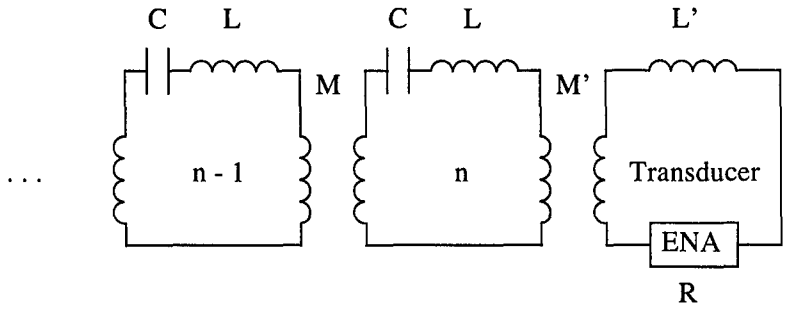

a)

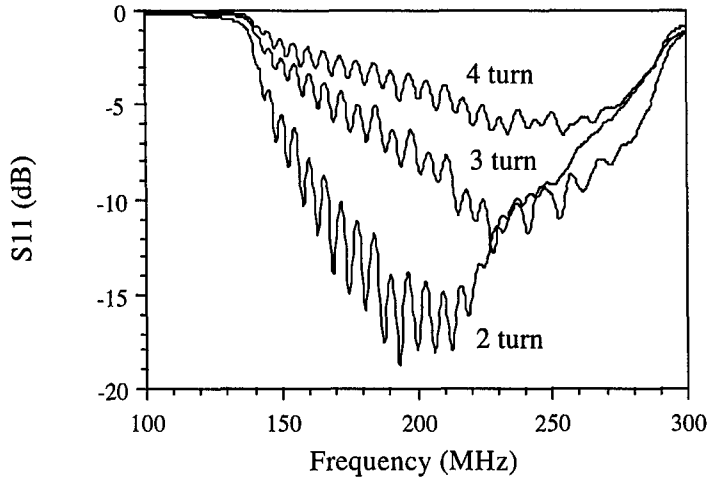

b)

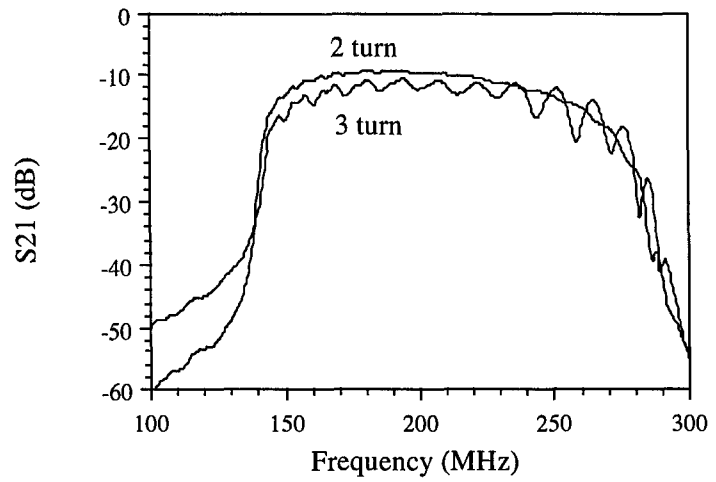

c)

Figure 18. a) Equivalent circuit of transducer; b) and c) frequency variation of S_{11} and S_{21}, for MI waveguides based on five-turn self-resonant "solenoidal" coils with an axial spacing of 3 mm, and planar coil transducers with different numbers of turns.

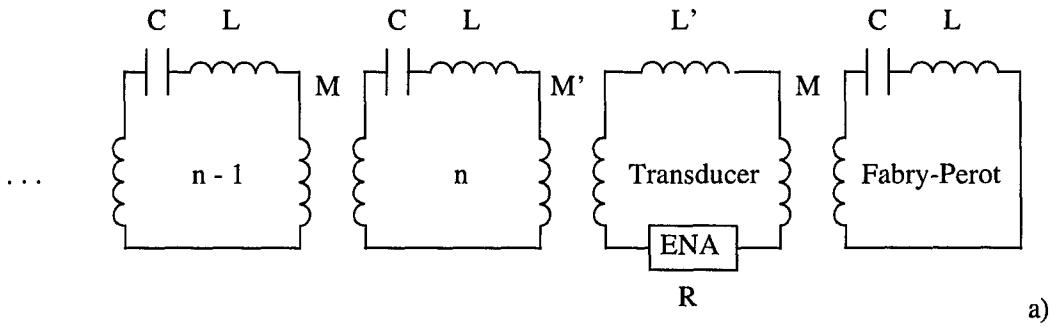

a)

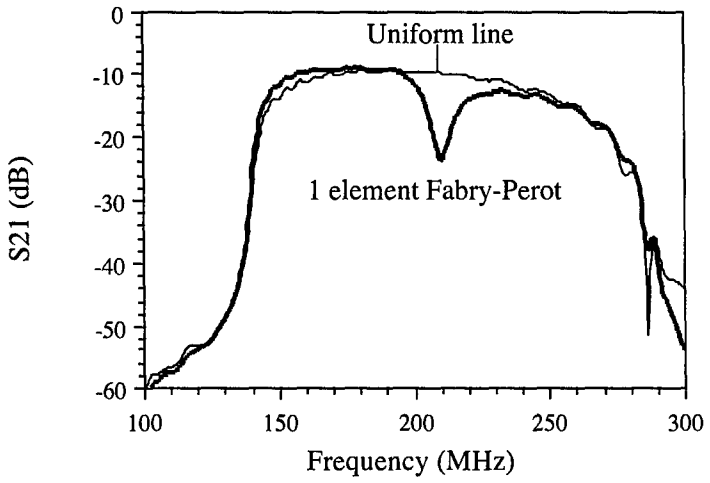

b)

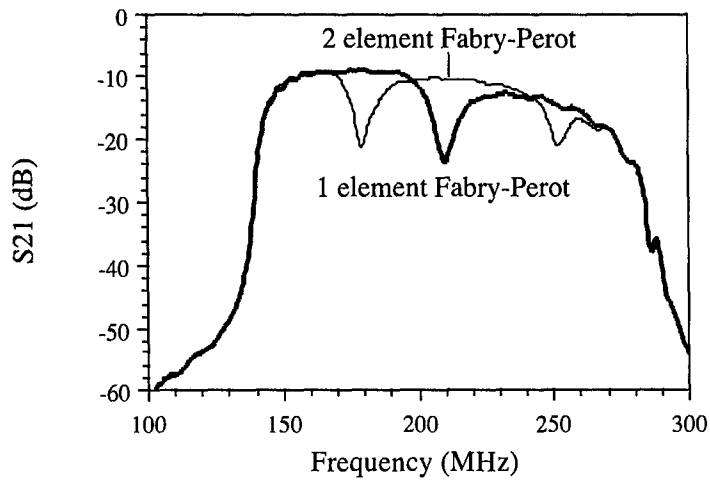

c)

Figure 19. Equivalent circuit of 1-element Fabry-Perot cavity; b) and c) frequency variation of S_{21} for MI Fabry-Perot resonators with one and two elements in the cavity.